A&A 398, 517–524 (2003)
DOI: 10.1051/0004-6361:20021672

Astronomy & Astrophysics

Non-Keplerian rotation in the nucleus of NGC 1068: Evidence for a massive accretion disk?

G. Lodato[1] and G. Bertin[2]

[1] Scuola Normale Superiore, Piazza dei Cavalieri 7, 56126 Pisa, Italy
[2] Università degli Studi di Milano, Dipartimento di Fisica, via Celoria 16, 20133 Milano, Italy

Received 9 September 2002 / Accepted 4 November 2002

Abstract. The nucleus of the Seyfert galaxy NGC 1068 is believed to host a supermassive black hole. Evidence for the presence of a massive central object is provided by water maser emission, which displays a linear pattern in the sky, suggestive of a rotating disk. The rotating disk hypothesis is further strengthened by the declining shape of the derived rotation curve. Similar maser emission from NGC 4258 has led to a reliable estimate of the mass of the central black hole, because in this case the rotation curve is Keplerian. In the case of NGC 1068 the rotation curve traced by the water maser is non-Keplerian. In this paper we provide an interpretation of the non-Keplerian rotation in NGC 1068 by means of a self-gravitating accretion disk model. We obtain a good fit to the available data and derive a black hole mass $M_\bullet \approx (8.0 \pm 0.3) \times 10^6\ M_\odot$. The resulting disk mass is comparable to the black hole mass. As an interesting by-product of our fitting procedure, we are able to estimate the viscosity parameter, which turns out to be $\alpha \approx 10^{-2}$, in line with some theoretical expectations.

Key words. accretion, accretion disks – galaxies: active – galaxies: individual: NGC 1068 – galaxies: kinematics and dynamics

1. Introduction

There is now convincing evidence that most AGNs host a supermassive black hole, with masses ranging from $10^7\ M_\odot$ to $10^9\ M_\odot$. The gravitational energy extracted from an accretion disk around such black holes is generally considered to be the main source of the AGN luminosity. Determining the mass of the central black hole $M_\bullet$ is thus one important goal of studies of AGNs. This has received greater attention recently, in a more general context, because correlations have been found between $M_\bullet$ and the global properties of the host galaxy, such as its mass or luminosity (Magorrian et al. 1998) or its central velocity dispersion (Ferrarese & Merritt 2000; Gebhardt et al. 2000a).

The central point mass $M_\bullet$ can be measured by different methods. The analysis of *HST* optical spectra in terms of stellar dynamical models (see, for example, Gebhardt et al. 2000b) and the study of gas kinematics from *HST* spectra (van der Marel & van den Bosch 1998) probe the nuclear gravitational field of nearby galaxies at distances typically of the order of ≈100 pc from the center. $M_\bullet$ can be estimated also from reverberation mapping of the broad line region, which is able to probe the gravitational field at smaller scales. However, reverberation mapping is not applicable to Type II Seyfert galaxies, like NGC 1068, in which the broad line region is hidden from our line of sight. An independent powerful tool to obtain reliable estimates of $M_\bullet$ is provided by the study of the Doppler shift of water maser emission lines (when available). This latter method provides the most reliable determinations of $M_\bullet$, because it probes the gravitational field at very small distances (less than 1 pc) from the center. The masing spots are often observed to trace a linear structure and show a declining rotation curve. In the case of NGC 4258 (Miyoshi et al. 1995), the rotation curve is remarkably Keplerian and leads to a robust determination of $M_\bullet \approx 3.9 \times 10^7\ M_\odot$.

NGC 1068 is one of the best studied Seyfert galaxies. It is considered to be the prototypical Type II Seyfert, in which the central engine is believed to be hidden from our line of sight by a dusty structure. This obscuring structure, now resolved with VLBA radio continuum observations (Gallimore et al. 1997), appears to have a disk-like rather than a toroidal shape. The bolometric luminosity of the nucleus is $L_{\rm bol} \approx 8 \times 10^{44}$ erg/s (Pier et al. 1994). If we adopt for the accretion efficiency a value of $\eta = 0.06$, appropriate for a non-rotating black hole, the resulting mass accretion rate is $\dot{M} \approx 0.235\ M_\odot$/yr. Throughout this paper we will assume that the distance to NGC 1068 is 14.4 Mpc (so that 1 mas = 0.069 pc).

Water maser emission is observed from the nucleus of NGC 1068 extending out to a radius $r \approx 1$ pc (Greenhill et al. 1996; Greenhill & Gwinn 1997). This emission is believed to

Send offprint requests to: G. Lodato, e-mail: lodato@sns.it

come from a rotating, almost edge-on accretion disk, possibly associated with the disk seen in VLBA continuum (Gallimore et al. 1997). The striking feature of this maser emission is that, in contrast with the case of NGC 4258, the rotation curve of the masing spots is clearly *non-Keplerian*. Greenhill et al. (1996) report a best fit to the data with a circular velocity $V \propto r^{-0.31}$. Possible causes for the sub-Keplerian rotation may be: a) the maser may not be associated with a pure rotating structure, because an outflow is present; b) radiation pressure may reduce the rotational velocity (Pier & Krolik 1992a); c) the source of the gravitational field may be extended, including a nuclear stellar cluster (as proposed by Kumar 1999) or the accretion disk itself.

In this paper we interpret the non-Keplerian rotation in NGC 1068 in terms of a self-gravitating accretion disk model (Bertin & Lodato 1999, hereafter BL). The disk is assumed to be self-regulated at the threshold of Jeans instability. The gravitational field is computed by solving the relevant Poisson equation including both the central point-like object and the disk. The resulting rotation curve is characterized by an inner Keplerian curve connected with an outer asymptotically flat rotation curve.

We have fitted the Very Long Baseline Interferometry (VLBI) data of Greenhill & Gwinn (1997) with our theoretical models. The fit is very good. From the results of the fit we can derive the value of the central black hole mass, $M_\bullet \approx 8 \times 10^6\ M_\odot$, roughly one half of the value that would be inferred from a Keplerian fit (from which one would obtain $M_\bullet \approx 1.5 \times 10^7\ M_\odot$), basically because we attribute part of the gravitating mass to the disk. As an interesting by-product of our modeling procedure, we are able to derive the value of the viscosity parameter α that regulates the accretion process, which turns out to be in agreement with some theoretical expectations.

The paper is organized as follows. In Sect. 2 we describe the role played by the disk self-gravity in the outer parts of AGNs. In Sect. 3 we report the observations of the nucleus of NGC 1068, focusing on its geometry and kinematics. In Sect. 4 we describe our fit to the water maser data. In Sect. 5 we discuss some possible alternatives to the model presented in this paper. In Sect. 6 we draw our conclusions. In Appendix A we describe in some detail the statistical significance of the fitting procedure adopted.

2. Preliminary considerations on the influence of the disk self-gravity in AGN accretion disks

The disk self-gravity may affect several aspects of the dynamics of accretion disks: a) gravitational instabilities are expected to modify the energy and angular momentum transport in the disk, perhaps being the main tool able to drive accretion at large radii (Lin & Pringle 1987); b) the vertical gravitational field associated with the disk modifies the vertical hydrostatic equilibrium (Paczyński 1978; Bardou et al. 1998); c) the radial gravitational field of the disk may lead to deviations from Keplerian rotation (BL).

2.1. Self-regulation of Jeans instability

The onset of gravitational instabilities in a fluid disk is controlled by the well-known axisymmetric stability parameter Q:

$$Q = \frac{c_s \kappa}{\pi G \sigma}, \tag{1}$$

where c_s is the thermal speed, κ is the epicyclic frequency, and σ is the disk surface density. For $Q < 1$ the disk is unstable. As Q is proportional to the thermal speed, a hot enough disk is expected to be free from the effects related to the disk self-gravity, while, on the other hand, if the disk is cold enough to begin with, it cannot survive long in such a condition and is likely to be eventually characterized by a value of Q close to unity, as a result of a self-regulation mechanism, studied and recognized especially in the field of galactic dynamics (see Bertin & Lin 1996). Self-regulation has been sometimes taken into account also in the context of accretion disks (Lin & Pringle 1987; Huré 2000). The inner parts of the accretion disk in AGNs are very hot, so that the disk self-gravity is not expected to play a role there. On the other hand, it is easy to show that the outer colder parts of the disk may be subject to gravitational instabilities. Consider the outer region of the α-disk solution by Shakura & Sunyaev (1973), for the case in which gas pressure and free-free absorption dominate. The radial dependence of Q in this case is:

$$Q \approx 5.6 \times 10^3 \alpha^{7/10} \dot{M}_{26}^{-11/20} M_8^{-3/4} \hat{r}^{-9/8}, \tag{2}$$

where we have scaled the basic physical parameters to typical AGN values, so that $\dot{M}_{26}$ is the mass accretion rate in units of 10^{26} g/s $\approx 1.57\ M_\odot$/yr, M_8 is the black hole mass in units of $10^8\ M_\odot$, and $\hat{r}$ is the radius in units of the Schwarzschild radius of the black hole $R_\bullet = 2GM_\bullet/c^2$; α is the dimensionless viscosity parameter entering the Shakura-Sunyaev prescription for viscosity. The value of Q thus decreases rapidly with increasing radius and becomes equal to unity at $\hat{r}_Q = r_Q/R_\bullet \approx 10^3$ (for $M_8 = \dot{M}_{26} = 1$ and $\alpha = 0.01$), i.e. at $r_Q \approx 10^{-2}$ pc. Kumar (1999) has carried out a similar analysis in the case in which the opacity is dominated by metal grains and has basically confirmed the above estimate, finding that $Q \approx 1$ at $r_Q \approx 3 \times 10^{-3}$ pc, for the same input parameters.

The argument of self-regulation suggests that the outer disk, beyond r_Q, be characterized by $Q \approx 1$.

2.2. Impact of the disk self-gravity on the vertical structure

If we consider the modifications of the vertical hydrostatic equilibrium by the disk self-gravity, a simple way to address the problem is to compare the vertical lengthscales derived in the limiting cases of non-self-gravitating disk and of fully self-gravitating disk. In the non-self-gravitating case we have:

$$h_{\rm nsg} = \frac{c_s}{\Omega}, \tag{3}$$

while in the self-gravitating case:

$$h_{\rm sg} = \frac{c_s^2}{\pi G \sigma}. \tag{4}$$

The disk self-gravity will then modify the vertical structure of the disk if:

$$\frac{h_{\rm sg}}{h_{\rm nsg}} = \frac{c_{\rm s}\Omega}{\pi G\sigma} \approx Q \approx 1, \tag{5}$$

because κ is related to Ω by a numerical factor (dependent on the rotation curve) close to unity. Therefore, a discussion of the vertical equilibrium also leads to the conclusion that an accretion disk is expected to be self-gravitating if it extends to radii larger than r_Q. This simplified analysis is confirmed by the more detailed study presented earlier by us (BL, Appendix), where a convenient analytical expression for the disk thickness, in the case in which both the disk and the central object are taken into account, is provided:

$$h = \frac{c_{\rm s}^2}{\pi G\sigma}\frac{\pi}{4Q^2(2\Omega^2/\kappa^2-1)} \times\left[\sqrt{1+\frac{8}{\pi}Q^2\left(\frac{2\Omega^2}{\kappa^2}-1\right)}-1\right]. \tag{6}$$

2.3. Modification of the rotation curve

In this paper we will refer to the self-gravitating steady-state disk model of BL, who considered disks that are self-regulated with respect to Jeans instability, so that $Q = \bar{Q} \approx 1$. The gravitational field of the disk is computed by solving self-consistently the relevant Poisson equation (see Eq. (4) of BL).

The basic dynamical feature of such self-regulated disk model is that at large radii the rotation curve $V(r)$ departs from the Keplerian profile, approaching an asymptotically flat rotation curve. The typical lengthscale that marks the transition from Keplerian to self-gravitating regime is:

$$r_{\rm s} = 2GM_\bullet\left(\frac{\bar{Q}}{4}\right)^2\left(\frac{G\dot{M}}{2\alpha}\right)^{-2/3}. \tag{7}$$

Deviations from Keplerian rotation occur already at radii of the order of a fraction of $r_{\rm s}$; in fact, we can have $\mathrm{d}\ln V/\mathrm{d}\ln r = -0.4$ at $r = 0.1r_{\rm s}$. For $r \gg r_{\rm s}$, the mass of the disk grows linearly, and the surface density behaves as $\sigma \propto 1/r$. If we estimate the value of $r_{\rm s}$, assuming the typical AGN values for the relevant parameters used earlier ($M_8 = \dot{M}_{26} = 1$ and $\alpha = 0.01$), we find that $r_{\rm s}$ is of the order of a few pc. Interestingly, we find that deviations from Keplerian rotation are expected to occur exactly at a distance from the center probed, in the case of NGC 1068, by the water maser emission. In contrast, in the case of NGC 4258, a similar analysis would lead to an estimated $r_{\rm s} \gg 1$ pc, consistent with the Keplerian rotation curve observed by Miyoshi et al. (1995).

Based on the arguments presented in this section, we therefore conclude that, if the water maser emission from NGC 1068 traces the outer parts of the nuclear accretion disk, such disk is likely to be self-gravitating for what concerns its vertical structure and transport phenomena, and it should display significant deviations from Keplerian rotation.

3. The masing spots in NGC 1068: Geometry and kinematics

In this section we will discuss the geometry of the maser emission in NGC 1068, for which different interpretations have been given.

3.1. Disk or torus?

Greenhill et al. (1996) observed the "red-shifted" water maser emission from NGC 1068, finding that it traces a linear pattern in the plane of the sky, inclined by approximately 45° with respect to the direction of the radio jet. The misalignment between the radio axis and the maser emission led to an early interpretation of the maser spots as arising from the upper limb of a nearly edge-on torus, characterized by a rather large aspect ratio (see the schematic representation in Fig. 1). According to this interpretation, we would expect that the corresponding "blue-shifted" emission should come from the dashed region shown in Fig. 1. On the other hand, subsequent observations (Greenhill & Gwinn 1997) showed that the emission traces a linear pattern from the "red-shifted" to the "blue-shifted" emission, hence arguing in favor of a thin disk interpretation. The misalignment between the disk axis and the radio jet is not uncommon in AGNs (see Schmitt et al. 2002) and may be due to a variety of physical mechanisms (for example, a warp in the outer disk; Pringle 1997).

3.2. Geometry of the disk emission

The rotation curve of the maser spots can be divided in two different regions: 1) at small impact parameter the masers show an apparently rising rotation curve; 2) starting from a radial distance ≈0.6 pc from the center the rotation curve declines, following a sub-Keplerian profile.

The natural interpretation of the declining part of the rotation curve is that it arises from material that moves parallel to our line of sight (i.e. that lies on a disk diameter perpendicular to the line of sight). The best argument in favor of this interpretation is that maser amplification is largest for material that lies close to the line of the nodes. On the other hand, the rising part of the observed "rotation curve" is thought to originate from one quarter of the disk at the inner maser disk radius, so that the rising curve is an effect of velocity projection along the line of sight (see also Miyoshi et al. 1995). According to this interpretation, the inner radius of the maser disk is located at ≈0.6 pc and the outer disk radius is at ≈1 pc.

Baan & Hashhick (1996) claimed to have observed a drift in the velocity of the water masers, indicating that the maser spots are subject to large accelerations, incompatible with the disk interpretation, according to which the maser centripetal acceleration should be perpendicular to the line of sight. Those large accelerations have not been confirmed by subsequent work by Gallimore et al. (2001), who, monitoring the velocity drift, find that the maser spots between 0.6 pc and 1 pc should lie within $\theta \lesssim 2°$ from the line of nodes.

In the following we will therefore assume that the water maser emission comes from an edge-on thin disk extending

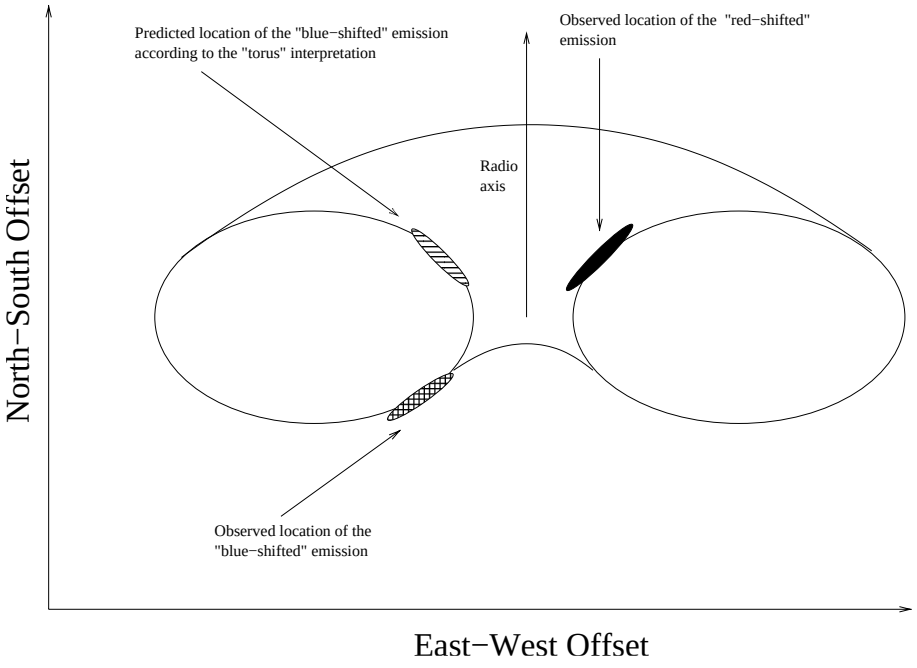

Fig. 1. Schematic representation of the location of the maser emission according to the torus interpretation. The three elliptical patches show the location of the observed "red-shifted" masers, of the predicted "blue-shifted" emission, based on the torus interpretation, and of the observed "blue-shifted" emission (see also Greenhill et al. 1996).

from 0.6 pc to 1 pc and that the declining part of the rotation curve comes from material that lies within 2° from the line of nodes.

4. Non-Keplerian rotation as an effect of the disk self-gravity

4.1. Fit procedure and results

Here we will fit the kinematical data of NGC 1068 by using the completely self-regulated disk model of BL (in which, for simplicity, the self-regulation prescription is taken to hold at all radii). Actually, we expect the inner disk to be hotter and characterized by a higher value of the stability parameter Q, so that a partially self-regulated disk model (also described in BL) would be more appropriate. In Sect. 4.3 we will justify the consistency of the simpler model adopted below.

The rotation curve of the completely self-regulated model by BL is determined when one specifies the radial lengthscale r_s (defined in Eq. (7)), the velocity scale V_0, defined as:

$$V_0^2 = \frac{8}{\bar{Q}^2}\left(\frac{G\dot{M}}{2\alpha}\right)^{2/3}, \tag{8}$$

and a dimensionless parameter (called ξ), which is proportional to the net angular momentum flux in the disk $\dot{J}$. We will fix this parameter by requiring the no-torque condition at the radius corresponding to the innermost stable orbit around the black hole. However, the specific choice of ξ is not critical for our conclusions, because we are exploring the disk properties at large radii, where the effects of the inner boundary condition are negligible. Therefore, we are left with two free dimensional scales, that are obtained by fitting the available data (from Greenhill & Gwinn 1997).

Note that, from the definitions of r_s and V_0, we have that:

$$V_0^2 = \frac{GM_\bullet}{r_s}. \tag{9}$$

Therefore, from the value of r_s and V_0 we can estimate $M_\bullet$ and $\dot{M}/\alpha$. In addition, once these quantities are specified, from the models of BL we can obtain the disk mass.

In our fit, we have restricted our attention to the data of the declining part of the rotation curve of the "red-shifted" maser (i.e. the data points with $r > 0.6$ pc), because these data are directly related to the gravitational potential. In contrast, the velocity data points at $r < 0.6$, according to the interpretation of the masing disk geometry presented in Sect. 3.2, only reflect the rotation at the inner radius of the masing disk and do not carry any additional information about the mass distribution. We have assumed that the systemic velocity is 1126 km s^{-1} (Greenhill & Gwinn 1997). The uncertainty in the position of the maser spots in the Greenhill & Gwinn (1997) data is of the order of $\approx 50\,\mu$as. The spectral resolution of the VLBI data is $\lesssim 1$ km s^{-1}. However, the velocity uncertainty ΔV is expected to be higher due to the uncertainties in the estimate of the systemic velocity and of the magnitude of turbulent motion in the disk. We will assume that these uncertainties sum up to ≈ 10 km s^{-1} (see also discussion in Appendix A). All fits are obtained with a χ-square minimization. The result of the fit, shown in Fig. 2, is satisfactory. The resulting reduced χ-square is $\tilde{\chi}^2 = 0.55$, with 48 degrees of freedom. The fit parameters are $V_0 = (110.4 \pm 0.3)$ km s^{-1} and $r_s = (2.82 \pm 0.1)$ pc, where the uncertainties define the 68% confidence level and are derived from the Hessian of the χ-square. The resulting black hole mass is $M_\bullet = (8.0 \pm 0.3) \times 10^6\ M_\odot$ and the disk mass is approximately equal to the black hole mass. We also obtain $\dot{M} = (28.1 \pm 0.2)\,\alpha\ M_\odot$/yr. If we estimate $\dot{M}$ from the bolometric luminosity (assuming an accretion efficiency $\eta = 0.06$), we obtain $\alpha \approx 8.3 \times 10^{-3}$, a reasonable number.

The best-fit curve resulting from the self-gravitating disk model is not a power-law. However, Greenhill et al. (1996) were able to obtain a good fit to the data by assuming a rotation curve of the form $V \propto r^{-0.31}$. If we compute the quantity

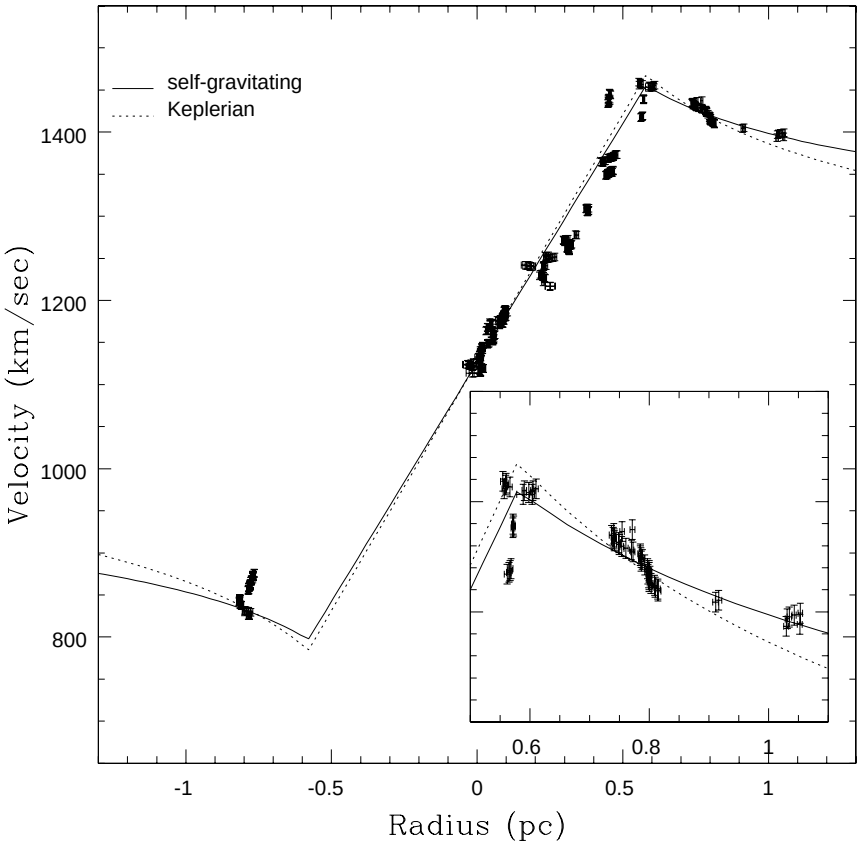

Fig. 2. Fit to the rotation curve from the water maser emission by a self-gravitating accretion disk model. Data from Greenhill & Gwinn (1997). The small panel shows a blow up of the declining part of the rotation curve together with the best fit obtained by assuming Keplerian rotation. The error bars reported here include uncertainties beyond the actual VLBI spectral resolution (see text).

d ln$V$/d ln$r$ for our best fit model, we find that it ranges from -0.35 at the inner edge of the disk to -0.30 at the outer edge.

We have also performed a fit by assuming a Keplerian rotation curve. The quality of the fit is definitely worse. The minimum χ-square in this case is in fact $\tilde{\chi}^2 = 1.557$ and is formally rejected at the 95% confidence level. The small panel of Fig. 2 compares the two models: the Keplerian best-fit curve fails to reproduce both the highest and the lowest part of the rotation curve. The resulting best-fit value of the black hole mass in the Keplerian fit is $M_\bullet \approx (1.50 \pm 0.02) \times 10^7\, M_\odot$. Note that the total mass (disk + black hole) of our self-gravitating best fit model is roughly the same as the black hole mass of the Keplerian fit. Therefore, a non-self-gravitating fit, which attributes all the mass to the central object, gives the correct value for the total mass, but fails to provide the correct slope of the rotation curve.

One consequence of the smaller value of the black hole mass derived from the self-gravitating disk model is that the corresponding Eddington luminosity of the black hole is proportionally reduced, hence leading to a higher Eddington ratio for the observed central object. In fact, based on the results of our fit, we derive that $L_{\rm bol}/L_{\rm Edd} = 0.77$, to be compared to the value $L_{\rm bol}/L_{\rm Edd} = 0.41$ obtained from the Keplerian fit. Note, however, that the Eddington luminosity is not well defined when the mass is not spherically distributed.

Some data points (at approximately 0.8 pc from the center) are not well fitted by neither the self-gravitating nor the Keplerian model. The velocities of these points display a higher slope with respect to that predicted by the best fit model. This discrepancy could be due to the fact that the corresponding masing spots lie on a spiral arclet, on a pattern not perfectly perpendicular to our line of sight, therefore leading to a smaller projected velocity.

The statistical significance of the above results, and in particular of the uncertainties on the parameters derived from the fit, depends on the assumed uncertainty in the observed velocities, which may not be easy to estimate. In Appendix A we discuss in detail this dependence and how to discriminate between the different models.

4.2. Properties of the best-fit disk model

Figure 3 shows the main physical properties of the best-fit disk model: the surface density profile, the cumulative mass, the equivalent thermal speed, and the aspect ratio (h/r), as derived from the self-regulated disk models of BL. The cumulative disk mass inside the outer radius of the disk is $M_{\rm disk}(r_{\rm out}) \approx (8.6 \pm 0.6) \times 10^6\, M_\odot$. Note that at large radii $\sigma \propto 1/r$ (also apparent from the approximately linear growth of the cumulative mass), with significant deviations at $r \lesssim 0.6$ pc. The equivalent thermal speed of the self-regulated model is approximately constant at large radii, as expected. The number density of H_2 molecules in the outer disk is in the range $1 - 5 \times 10^8$ cm^{-3}, compatible with the conditions for maser emission and consistent with models of circumnuclear gas heated by the AGN (Neufeld et al. 1994; Pier & Voit 1995). X-ray observations (Bianchi et al. 2001) and VLBA radio continuum observations (Gallimore et al. 1997) provide lower limits for the *electron* number density in the disk/torus to be $n_{\rm e} \gtrsim 3 \times 10^5$ cm^{-3}, and $n_{\rm e} \gtrsim 10^{6.8}$ cm^{-3}, respectively.

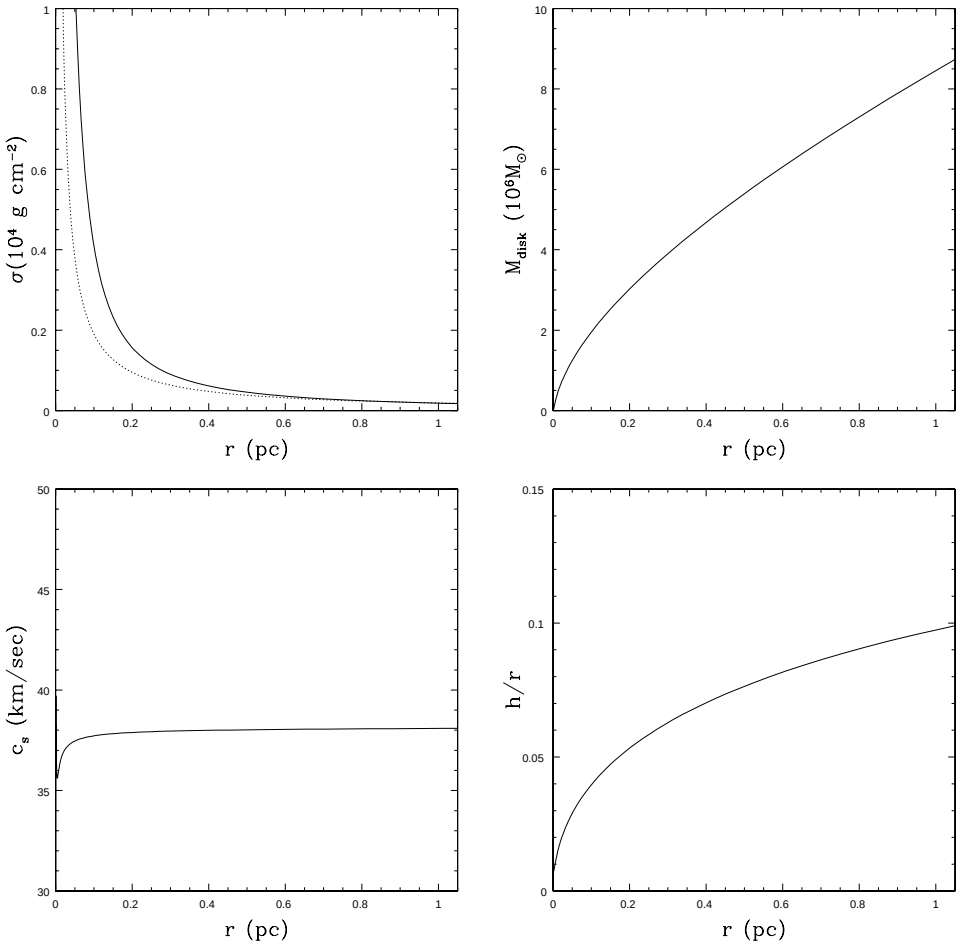

Fig. 3. Surface density profile (*upper left*), cumulative mass (*upper right*), equivalent thermal speed (*lower left*), and aspect ratio (*lower right*) of the best-fit accretion disk model to the maser data of NGC 1068. The dotted line in the surface density plot is the curve with $\sigma \propto 1/r$ that matches the asymptotic behavior at large radii.

4.3. Consistency of the self-regulated disk assumption

Starting from Eq. (2), we can compute the radius at which Q is expected to become of the order of unity in a non-self-gravitating model. If we refer to the physical parameters found from the fit in the previous section (i.e., $M_\bullet = 8 \times 10^6\ M_\odot$, $\alpha = 8.3 \times 10^{-3}$, and $\dot{M} = 0.23\ M_\odot$/yr), we find $r_Q \approx 10^{-3}$ pc. The onset of the self-regulation mechanism is therefore expected to take place very deep inside the disk, with respect to the radial distances on which we focus here, so that the use of a simple completely self-regulated model made in the previous Section is justified.

To strengthen this argument, we have also perfomed a fit by assuming the partially self-regulated disk model, described in BL, in which the profile of the stability parameter Q is assumed to decrease according to Eq. (2) for $r \ll r_Q$ and to be flat at $r \gg r_Q$, with $r_Q = 10^{-3}$ pc. No significant differences are found with respect to the completely self-regulated case.

5. Alternative scenarios

In this Section we discuss some possible models, alternative to the self-gravitating disk picture, developed to explain the non-Keplerian curve in NGC 1068. In particular, we will concentrate on the effect of a nuclear stellar cluster and on the effect of radiation pressure. Other models also exist (for example, the effect of a warp in the disk), but have been discussed in the literature less frequently.

5.1. Nuclear stellar concentration

One possibility is that the non-point-like source of gravitational field be distributed spherically rather than in a disk. A spheroidal nuclear stellar cluster, for example, could produce significant changes to the rotation curve traced by water maser emission, if its mass enclosed within 1 pc from the central engine exceeds $10^7\ M_\odot$ (Kumar 1999).

Indeed, a nuclear cusp in the luminosity profile has been observed in NGC 1068 (Thatte et al. 1997). Based on stellar velocity dispersion measurements, Thatte et al. (1997) estimate the dynamical mass within 1″ (≈69.8 pc at a distance of 14.4 Mpc) to be $\approx 6 \times 10^8\ M_\odot$. Schinnerer et al. (2000) report a value of $10^8\ M_\odot$ within a 25 pc diameter from the center, based on CO kinematics. It should be noted, however, that these mass estimates cannot be associated with the stellar cluster only, as the observed kinematics includes also the contributions of the central black hole and of the disk to the gravitational field.

Kumar (1999) has extrapolated the mass profile down to small radii of the order of 1 pc from the central engine of NGC 1068 starting from the mass estimate of Thatte et al. (1997) and assuming that the stellar cluster can be described as a singular isothermal sphere, with stellar density $\rho \propto r^{-2}$. In this case, the resulting mass enclosed in 1 pc would be $\approx 8.6 \times 10^6\ M_\odot$, therefore able to reproduce the desired deviations from Keplerian rotation. However, this procedure overestimates the stellar contribution in the inner regions, because the stellar cluster is not expected to be characterized by the singular isothermal sphere profile down to the innermost regions. Empirically, shallower profiles are generally found (Faber et al. 1997). In addition, the adiabatic growth of a black hole at the center of a stellar cluster leads to a density profile $\rho \propto r^{-3/2}$ (Cipollina & Bertin 1994) inside the radius of influence of the black hole $r_{\rm bh} = GM_\bullet/\sigma_\star^2$, where $\sigma_\star$ is the stellar velocity dispersion (curiously, if we use the value of $\sigma_\star$ provided by Thatte et al. 1997, we find that $r_{\rm bh}$ is of the order of a few parsec, comparable to the scales at which the maser emission is observed in NGC 1068). Recent N-body simulations of the formation of galactic nuclei by merger of two galaxies with initially steep density profiles ($\rho \propto r^{-2}$) (Milosavljević & Merritt 2001) have shown that a shallow stellar cusp is left around the nucleus, with $\rho \propto r^{-1}$ inside a break radius of the order of 10^2 pc.

Another difficulty with the picture of a compact stellar cluster is based on dynamical arguments. A collisional timescale for a stellar system characterized by a velocity dispersion $\sigma_\star$ and density ρ is given by:

$$t_{\rm coll} = \frac{\sigma_\star^3}{8\pi G^2 \rho m \ln\Lambda}, \tag{10}$$

where m is the stellar mass and $\ln\Lambda$ is the Coulomb logarithm (we will assume $\ln\Lambda = 10$). The nuclear stellar cluster should have at least a density of $\rho = 10^7\ M_\odot/{\rm pc}^3$ in its inner regions. If we assume $\sigma_\star = 150\ {\rm km\,s^{-1}}$, the value reported by Thatte et al. (1997), and a stellar mass $m = M_\odot$, we obtain $t_{\rm coll} \approx 6.5 \times 10^7$ yrs. Therefore, the nuclear stellar cluster, at the high densities required to modify the rotation curve, will be subject to collisional effects, that may lead to the rapid dynamical evolution of the stellar cluster itself.

To derive firm conclusions about the effect of the stellar central concentration on the water maser rotation curve, a more detailed knowledge of the properties of the cluster at the smallest scales is needed.

5.2. Radiation pressure support

Based on radiative transfer models of a thick torus (Pier & Krolik 1992a,b), it has been shown that radiation pressure may reduce the importance of the gravitational field of the central object. The relative importance of this effect changes at different radii inside the torus and could in principle lead to a modification of the rotation curve. The main drawback of this picture is that radiation pressure is also very efficient at reducing the vertical gravitational field. Therefore, we would expect the disk to be rather thick, against the observational evidence that the water maser emission lies in a geometrically thin structure. In fact, the model of Pier & Krolik (1992a) was intended to give a theoretical framework for the existence of thick tori in AGNs. A more detailed investigation of the effect of radiation pressure on thin configurations would therefore be needed to assess the importance of this process in the case of NGC 1068.

6. Conclusions

In this paper we have shown how the study of water maser emission in AGNs can be a very useful tool not only to estimate the central black hole mass, but also to study the properties of the associated accretion disk. In particular, we have described the non-Keplerian rotation curve in NGC 1068 in terms of a self-gravitating accretion disk, by fitting the data of Greenhill & Gwinn (1997) with the model described in Bertin & Lodato (1999). The quality of the fit is satisfactory and leads to $M_\bullet \approx M_{\rm disk} \simeq 8 \times 10^6\ M_\odot$. We have also estimated the long-sought value of the α viscosity parameter, obtaining $\alpha \approx 10^{-2}$.

Our study has additional interesting consequences. Previous estimates of $M_\bullet$, using a non-self-gravitating disk model, give $M_\bullet \simeq 1.5 \times 10^7\ M_\odot$, very close to the value of the total black hole + disk mass obtained by us. The reduced black hole mass obtained in the self-gravitating disk scenario leads to a reduced $L_{\rm Edd}$ for NGC 1068, so that the Eddington ratio turns out to be larger than previously thought. In fact, we obtain $L_{\rm bol}/L_{\rm Edd} \simeq 0.77$. More generally, it is important to derive firm results on $M_\bullet$ also in view of the correlations recently found between $M_\bullet$ and the global properties of the host galaxy, such as the $M_\bullet - \sigma_\star$ relation (Ferrarese & Merritt 2000; Gebhardt et al. 2000a). In this context, it is worth noting that the masses derived from water maser emission have been considered as the most reliable estimates; NGC 1068 is indeed one of the galaxies in the Gebhardt et al. (2000a) sample.

Acknowledgements. The authors wish to thank L. Greenhill for kindly providing the water maser data, R. Renò for illuminating discussions about statistical analysis, and J. Gallimore and M. Lombardi for interesting suggestions. This work has been partially supported by MIUR of Italy.

Appendix A: A likelihood ratio test for the self-gravitating disk model

As noted at the end of Sect. 4.1, the results of a statistical analysis of the water maser data depend significantly on the uncertainty assigned to the velocity data points. In this Appendix we examine this issue and discuss how it is connected with the general problem of discriminating between the Keplerian disk from the self-gravitating disk model. In fact, if the uncertainty in the velocities were sufficiently high, we would be unable to discriminate between the two different models.

The self-gravitating disk hypothesis is a generalization of the Keplerian one, to which it reduces when $M_{\rm disk} \to 0$ (or equivalently when $r_{\rm s} \to \infty$). Clearly, if the two models are fitted to the data, the minimum χ-square of the model with a larger number of parameters is going to be smaller. On the other hand, a well-known result of statistical analysis (see Eadie et al. 1971) enables us to compare two competing hypotheses in this

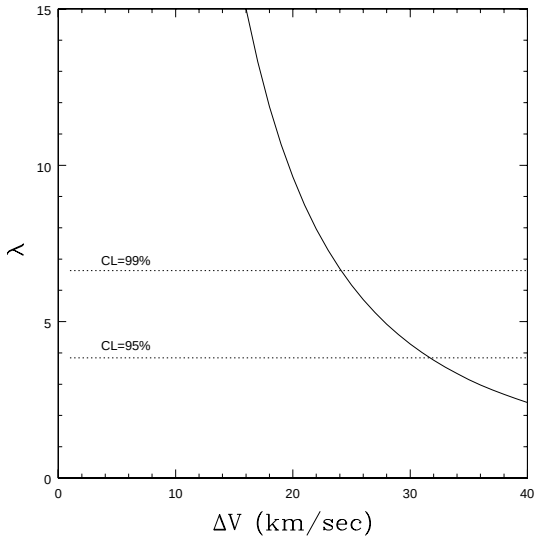

Fig. A.1. Likelihood ratio λ as a function of velocity uncertainty ΔV. The dotted lines indicate the 95% and the 99% confidence limits.

case. For Gaussian, independent measurements, the "likelihood ratio" λ, defined as:

$$\lambda = (\min\chi^2)_{\rm Kep} - (\min\chi^2)_{\rm sg}, \tag{A.1}$$

is distributed like a χ-square with n degrees of freedom, where n is the number of new parameters in the more general model (in our case $n = 1$), *under the hypothesis that the less general model is correct* (in our case, the Keplerian model). Of course, the resulting value of λ depends on the assumed uncertainties. Therefore, an interesting question is how large should the velocity uncertainty (for example, that associated with the magnitude of turbulent velocities) be to make the Keplerian hypothesis acceptable with respect to the self-gravitating one.

In Fig. A.1 the likelihood ratio λ is plotted as a function of the assumed velocity uncertainty ΔV. The two dotted lines define the 99% and 95% confidence limits. The figure clearly shows that the Keplerian model should be rejected against the self-gravitating one, with 99% confidence, if $\Delta V \lesssim 25$ km s^{-1}, and with 95% confidence, if $\Delta V \lesssim 30$ km s^{-1}. Note that the required uncertainty to make the Keplerian model acceptable is more than 20 times the formal instrumental uncertainty. This may be the reason why Greenhill & Gwinn (1997) argued that "the scatter in the data may indicate turbulent velocities of up to a few tens of km s^{-1}".

References

Baan, W. A., & Hashhick, A. 1996, ApJ, 269, 473
Bardou, A., Heyvaerts, J., & Duschl, W. 1998, A&A, 337, 966
Bertin, G., & Lin, C. 1996, Spiral Structure in Galaxies: A Density Wave Theory (Cambridge: MIT Press)
Bertin, G., & Lodato, G. 1999, A&A, 350, 694, (BL)
Bianchi, S., Matt, G., & Iwasawa, K. 2001, MNRAS, 322, 669
Cipollina, M., & Bertin, G. 1994, A&A, 288, 43
Eadie, W. T., Drijard, D., James, F. E., et al. 1971, Statistical Methods in Experimental Physics (London: North Holland)
Faber, S. M., Tremaine, S., Ajhar, E. A., et al. 1997, AJ, 114, 1771
Ferrarese, L., & Merritt, D. 2000, ApJ, 539, L9
Gallimore, J., Baum, S. A., & O'Dea, C. P. 1997, Nature, 388, 852
Gallimore, J., Henkel, C., Baum, S. A., et al. 2001, ApJ, 556, 694
Gebhardt, K., Bender, R., Bower, G., et al. 2000a, ApJ, 539, L13
Gebhardt, K., Richstone, D., Kormendy, J., et al. 2000b, AJ, 119, 1157
Greenhill, L., & Gwinn, C. 1997, Ap&SS, 248, 261
Greenhill, L., Gwinn, C. R., Antonucci, R., & Barvainis, R. 1996, ApJ, 472, L21
Huré, J. 2000, A&A, 358, 378
Kumar, P. 1999, ApJ, 519, 599
Lin, D., & Pringle, J. 1987, MNRAS, 225, 607
Magorrian, J., Tremaine, S., Richstone, D., et al. 1998, AJ, 115, 2285
Milosavljević, M., & Merritt, D. 2001, ApJ, 563, 34
Miyoshi, M., Moran, J., Herrnstein, J., et al. 1995, Nature, 373, 127
Neufeld, D. A., Maloney, P. R., & Conger, S. 1994, ApJ, 436, L127
Paczyński, B. 1978, Acta Astronomica, 28, 91
Pier, E. A., & Krolik, J. H. 1992a, ApJ, 399, L23
Pier, E. A., & Krolik, J. H. 1992b, ApJ, 401, 99
Pier, E., & Voit, G. M. 1995, ApJ, 450, 628
Pier, E., Antonucci, R., Hurt, T., Kriss, G., & Krolik, J. 1994, ApJ, 428, 124
Pringle, J. 1997, MNRAS, 292, 136
Schinnerer, E., Eckart, A., Tacconi, L. J., Genzel, R., & Downes, D. 2000, ApJ, 533, 850
Schmitt, H., Pringle, J. E., Clarke, C. J., & Kinney, A. L. 2002, ApJ, 575, 150
Shakura, N., & Sunyaev, R. 1973, A&A, 24, 337
Thatte, N., Quirrenbach, A., Genzel, R., Maiolino, R., & Tecza, M. 1997, ApJ, 490, 238
van der Marel, R. P., & van den Bosch, F. 1998, AJ, 116, 2220